GEOPHYSICS, VOL. 78, NO. 5 (SEPTEMBER-OCTOBER 2013); P. L87–L99, 11 FIGS., 2 TABLES.
10.1190/GEO2013-0074.1

Embedded-bound method for estimating the change in bulk modulus under either fluid or solid substitution

Gary Mavko[1] and Nishank Saxena[1]

ABSTRACT

Fluid and solid substitution of bulk modulus are exact and unique for materials whose elastic bulk and/or shear moduli fall on the Hashin-Shtrikman bounds. For materials whose moduli lie between the bounds, solid and fluid substitution of bulk moduli can be computed *exactly*, but not *uniquely*. Every initial bulk modulus can be realized with an infinite number of microstructures and therefore transform to an infinite number of moduli upon substitution of the pore fill. This nonuniqueness arises when detailed information on the material pore geometry is not available. We evaluated four embedded-bound constructions for fluid and solid substitution that were based on realizable materials. In the limiting case of pore fluids, two of these constructions reduced to the bounds of Gibiansky and Torquato, which illustrated that those bounds were optimum. For solids, the first two constructions corresponded to a homogeneous pore stiffness and predicted the smallest change in modulus. The third construction prediction corresponded to a pore space with heterogeneous stiffness, and it predicted a much larger change in modulus.

INTRODUCTION

Predicting the change of rock elastic properties upon substitution of the pore-filling material is one of the most fundamental problems in rock physics. Gassmann (1951) derives expressions for the change in rock effective elastic moduli when the pore-filling materials are *ideal fluids*. His results are stunningly simple and general under the assumptions that the empty frame of the rock is linear elastic, the solid phase (mineral) is homogeneous, the pore-filling material has the same load-induced pressure everywhere, and the shear stress within the fluid is zero everywhere.

Although Gassmann's results apply to arbitrary anisotropy, we limit the discussion in this paper to the isotropic case, in which the bulk modulus K and shear modulus G completely describe the rock's elasticity. In this case, Gassmann predicts

$$\frac{K_{\text{sat}}}{K_{\text{min}} - K_{\text{sat}}} = \frac{K_{\text{dry}}}{K_{\text{min}} - K_{\text{dry}}} + \frac{K_f}{\phi(K_{\text{min}} - K_f)}, \tag{1}$$

$$G_{\text{sat}} = G_{\text{dry}}, \tag{2}$$

where K_{dry} is the dry ("drained") rock effective bulk modulus, K_{sat} is the bulk modulus of the rock when fully saturated ("undrained") with an ideal fluid, K_{min} is the elastic bulk modulus of the mineral, K_f is the bulk modulus of the pore fluid, and ϕ is the porosity. In equation 2, G_{sat} and G_{dry} are the effective shear moduli of the saturated and dry rock, respectively, which are predicted to remain unchanged with substitution of the pore fluid. (Brown and Korringa [1975] extend Gassmann's derivation to the case of heterogeneous, though still linear elastic, mineralogy.)

The utility and simplicity of Gassmann's result come from its dependence on only a single average stiffness parameter of the dry pore space K_ϕ defined here as

$$\frac{1}{K_\phi} = -\frac{1}{\bar{v}_\phi}\frac{\partial \bar{v}_\phi}{\partial P_c}\bigg|_{P_p}, \tag{3}$$

where $\bar{v}_\phi$ is the total pore space volume, P_c is the confining pressure, and P_p is the pore pressure. The pore stiffness K_ϕ can be determined, for example, from dry rock measurements:

$$\frac{1}{K_\phi} = \frac{1}{\phi}\left(\frac{1}{K_{\text{dry}}} - \frac{1}{K_{\text{min}}}\right). \tag{4}$$

In terms of K_ϕ, one can rewrite equation 1 as (Mavko and Mukerji, 1995)

Manuscript received by the Editor 24 February 2013; published online 2 September 2013.
[1]Stanford University, Department of Geophysics, Rock Physics Laboratory, Stanford, California, USA. E-mail: mavko@stanford.edu; nishank@stanford.edu.

$$\frac{1}{K_{sat}} = \frac{1}{K_{min}} + \frac{\phi}{K_\phi + F}; \qquad F = \frac{K_f K_{min}}{K_{min} - K_f}. \tag{5}$$

An infinite number of connected pore microstructures exist that share the same K_{min}, K_{dry}, K_ϕ, and ϕ. Each will have exactly the same Gassmann-predicted response to pore-fluid change. The same *cannot* be said if the pores become filled with solids or viscoelastic materials or if the pore space becomes disconnected.

Solid substitution, rather than fluid substitution, applies, for example, when predicting how elastic moduli of heavy oil reservoirs change with saturation or upon heating or steam injection. Solid substitution is also necessary to model plugging of a pore space with cement or salt or removal of minerals during the formation of secondary porosity. Solid substitution takes place during alteration of feldspar to clay or when comparing clean pore space with clay-filled pores. Equations for solid substitution also allow predictions of changes in viscoelastic pore-filling materials, by virtue of the viscoelastic correspondence principle.

In this paper, we present techniques for computing the change in the effective bulk modulus of a rock upon substituting solids, liquids, or viscoelastic materials in the pore space. The approach is based upon recursive use of the Hashin-Shtrikman (1963) (HS) bounds for two-phase materials, which guarantees that the results are physically realizable. We reproduce the known result (Kanter and Bergman, 1984; Berryman and Milton, 1988) that the rock response to changes in (solid or fluid) pore fill is nonunique. The "embedded-bound" method reduces to the upper and lower bounds for *fluid* substitution developed by Gibiansky and Torquato (1998), illustrating that those bounds are optimum. Changes in the effective bulk modulus are smallest when the pore space is stiff and homogeneous and largest when the pore space is heterogeneous.

In this paper, we generalize the term "porosity" to mean the volume fraction of rock that is being substituted. When substituting one pore fluid for another, porosity has its usual meaning; when the pore space is completely filled with a mineral, we still refer to that volume fraction as porosity.

We present here results only for the effective bulk modulus of two-phase composites. Results for shear modulus will be presented in the future.

CIZ-SHAPIRO APPROXIMATION FOR SOLID PORE-FILL SUBSTITUTION

Ciz and Shapiro (2007) derive extensions of Gassmann's equations to the case of a *solid* pore-filling material. For an isotropic composite with homogeneous mineralogy, they offer the approximations,

$$\frac{K_{sat}}{K_{min} - K_{sat}} \approx \frac{K_{dry}}{K_{min} - K_{dry}} + \frac{K_f}{\phi(K_{min} - K_f)}, \tag{6}$$

$$\frac{G_{sat}}{G_{min} - G_{sat}} \approx \frac{G_{dry}}{G_{min} - G_{dry}} + \frac{G_f}{\phi(G_{min} - G_f)}, \tag{7}$$

where K_{sat} and G_{sat} are the effective bulk and shear moduli of the filled rock and K_f and G_f are the bulk and shear moduli of the pore-filling material (solid or fluid). In this paper, we will refer to equations 6 and 7 as the Ciz-Shapiro (C&S) approximation. (The C&S expressions follow from approximations to well defined but unknown parameters in their otherwise exact expressions for solid-substituted bulk and shear moduli.) Note that equations 6 and 7 reduce to Gassmann's fluid substitution equations when $G_f = 0$.

The C&S approximation of bulk modulus (equation 6) is valid in situations when there is no change to the pore-fill shear modulus upon solid substitution and when the first stress invariant $I_1 = \sigma_{kk}$ (i.e., trace of the stress tensor = 3 × mean stress) within the pore-filling material is homogeneous under hydrostatic loading. The stress tensor within the pore fill is homogeneous if and only if the composite bulk and shear moduli fall on the upper HS bounds (Milton, 1986; Torquato, 2001). In fact, equation 6 is derivable from the expressions for the upper HS bounds. The weaker condition that I_1 is homogeneous can be achieved between the bounds, as will be discussed later. The more general case of composites with heterogeneous induced mean stress under hydrostatic loading will experience larger changes in solid-substituted effective modulus than predicted by equation 6, for the usual case when the changes in pore-filling bulk and shear moduli have the same sign. We show with numerical examples that the C&S prediction works well if the pore space consists of a very dilute distribution of identical, randomly oriented ellipsoidal pores. Zou et al. (2010) present an extensive discussion of the strain heterogeneity within inclusions of a variety of shapes and the pitfalls of ignoring it.

Table 1 compares C&S predictions with modeled estimates of bulk and shear moduli in dry, fluid-filled, and solid-filled synthetic rocks. The pore spaces are composed of spheroidal inclusions, and the dry-rock effective moduli are estimated using the self-consistent (SC) approximation (Berryman, 1980). (The SC model approximates the strain within each pore with that of a single pore sitting in a homogeneous medium having moduli equal to the effective moduli being computed.) In these examples, the matrix mineralogy is assumed to be quartz (bulk modulus $K_{min} = 36$ GPa; shear modulus $G_{min} = 45$ GPa). In the first set of examples (rows a-d), the pores are all spherical. In the second set (rows e-g), all pores are identical, randomly oriented, penny-shaped cracks. In the third set (rows h-j), the pores are a dual-porosity mix of spherical pores and penny-shaped cracks. In each row, the pore-filled rock moduli are also estimated using the SC approximation, assuming the same pore geometry as the corresponding dry rock computation. The C&S solid-filled rock moduli are computed by applying equations 6 and 7 to the SC dry rock moduli. (It is important to remember that the SC model is also an approximation. It gives the most consistent dry-versus-pore-filled moduli at pore volume fractions much smaller than the corresponding pore aspect ratios.)

We observe the following by comparing the last two columns of Table 1:

1) Row a: fluid-filled spheres. The C&S-predicted moduli agree with the SC-predicted moduli (to at least three significant digits).
2) Rows b-d: solid-filled spheres. The C&S-predicted moduli are slightly smaller than the moduli predicted from the SC approximation. This could be in part from imperfections in the SC model, but also from ignoring coupling of the bulk and shear calculations in the C&S approximation.
3) Row e: fluid-filled identical cracks. SC and C&S bulk moduli agree to within <1%. The SC shear moduli are stiffer than the C&S predictions because SC assumes isolated pores, whereas the C&S assumes hydraulically connected pores.

4) Rows f-g: solid-filled identical cracks. The C&S moduli are up to 3% softer than the SC moduli. Hydraulic connectivity is not an issue because the pore fill is solid. The differences are primarily due to heterogeneity of pore strain that is ignored by the C&S approximation and the lack of coupling between the C&S bulk and shear calculations.
5) Row h: fluid-filled dual porosity. The SC moduli are very much stiffer than the C&S moduli due to the different assumptions about hydraulic connectivity.
6) Rows i-j: solid-filled dual porosity. The C&S moduli are systematically too soft, by as much as 30%.

These few examples suggest that the C&S approximation for bulk modulus is most appropriate for rocks with homogenous, equidimensional pores.

FLUID SUBSTITUTION ON THE BOUNDS

Hashin and Shtrikman (1963) and Walpole (1966) find expressions for bounds on the elastic bulk and shear moduli of an isotropic two-phase composite:

$$K^{\mathrm{HS}+/-} = K_1 + \frac{f_2}{(K_2 - K_1)^{-1} + f_1\left(K_1 + \frac{4}{3}G_m\right)^{-1}}, \quad (8)$$

$$G^{\mathrm{HS}+/-} = G_1 + \frac{f_2}{(G_2 - G_1)^{-1} + f_1\left(G_1 + \frac{G_m 9K_m + 8G_m}{6}\frac{K_m + 2G_m}{K_m + 2G_m}\right)^{-1}}, \quad (9)$$

where the subscripts 1 and 2 refer to the properties of the two phases. Equations 8 and 9 yield the upper bound when K_m and G_m are the maximum bulk and shear moduli of the individual phases, and they yield the lower bounds when K_m and G_m are the minimum bulk and shear moduli of the phases. We will refer to equations 8 and 9 as the HS bounds. Superscripts HS+ and HS− designate the upper and lower bounds, respectively.

It has been known for some time that the HS bounds on the elastic moduli of two-phase porous media are Gassmann consistent. That is, if the bulk modulus of a two-phase material, in which one of the phases is a fluid, falls on one of the HS bounds, then if the fluid is replaced by a second fluid, the modulus of the resulting composite remains on the bound. This was implied by the original derivation of Hashin and Shtrikman (1963), in which their trial stress and strain fields in the pore phase were constant (Gibiansky and Torquato, 1998); in the case of fluids, this means uniform pressure and zero shear stress in the pore space, which are equivalent to Gassmann's assumptions. The uniformity of the inclusion stress for microstructures attaining the bound is also pointed out, for example, by Gibiansky and Sigmund (2000). Yan and Han (2011) also discuss the consistency of the HS bounds with Gassmann's model. It is interesting that fluid-saturated two-phase media whose moduli fall on the bounds will be consistent with Gassmann fluid substitution, even if the pores are not connected.

BOUNDS ON FLUID SUBSTITUTION

When two-phase materials do not fall on the bounds, then fluid substitution may not be Gassmann consistent. In the geophysics literature, deviation from Gassmann's predictions has been extensively discussed in the context of load-induced unequilibrated pore pressure as occurs in disconnected pores or during unrelaxed "squirt flow" (Biot, 1962; Stoll and Bryan, 1970; Mavko and Nur, 1975; O'Connell and Budiansky, 1977; Mavko and Jizba, 1991; Chapman et al., 2002; Gurevich et al., 2009). Fluid substitution with unequilibrated pore fluids yields larger changes in bulk modulus than those predicted by Gassmann.

Table 1. Comparison of pore-filled moduli, using the SC approximation versus the C&S approximation. All pores are ellipsoidal. Frame minerals have bulk and shear moduli of 36 and 45 GPa. Minerals in the SC approximation have an aspect ratio = 1. First set, spherical pores; second set, identical oblate spheroids; third set, dual-porosity mix of spheres and oblate spheroids. Solid ($G_f > 0$) and liquid ($G_f = 0$) pore-filling materials are considered.

	Pore aspect ratios	Pore volume fractions	Infill K_f (GPa)	Infill G_f (GPa)	SC dry-rock K, G (GPa)	SC filled-rock K, G (GPa)	C&S filled K, G (GPa)
Spheres							
a)	1	0.1	2	0	30.1, 35.6	30.6, 35.6	30.6, 35.6
b)	1	0.1	2	2	30.1, 35.6	30.7, 36.5	30.6, 36.4
c)	1	0.1	10	10	30.1, 35.6	32.5, 39.3	32.4, 39.1
d)	1	0.2	10	10	23.9, 26.3	29.0, 33.9	28.6, 33.3
Identical cracks							
e)	0.01	0.01	2	0	22.8, 29.1	32.0, 33.6	31.9, 29.1
f)	0.01	0.01	2	2	22.8, 29.1	33.7, 41.3	31.8, 39.0
g)	0.01	0.01	10	10	22.8, 29.1	35.5, 44.1	35.1, 43.6
Dual porosity							
h)	[1, 0.01]	[0.09, 0.01]	2	0	18.3, 22.1	27.5, 26.6	22.3, 22.1
i)	[1, 0.01]	[0.09, 0.01]	2	2	18.3, 22.1	29.3, 34.4	22.3, 26.5
j)	[1, 0.01]	[0.09, 0.01]	10	10	18.3, 22.1	32.3, 39.0	29.9, 35.7

Gibiansky and Torquato (1998) discuss the nonuniqueness of fluid substitution and present rigorous bounds on the change in bulk modulus that can occur upon fluid substitution in a two-phase composite. If the initial effective bulk modulus is $K_{\text{sat}}^{(1)}$ when the rock is saturated with fluid of bulk modulus $K_f^{(1)}$, then upon substituting a new fluid with bulk modulus $K_f^{(2)}$, the new saturated effective bulk modulus $K_{\text{sat}}^{(2)}$ must lie in the interval,

$$F_1 \le K_{\text{sat}}^{(2)} \le F_2 \quad \text{if } K_f^{(2)} > K_f^{(1)}, \quad F_1 \ge K_{\text{sat}}^{(2)} \ge F_2 \quad \text{if } K_f^{(2)} < K_f^{(1)}, \tag{10}$$

where

$$F_1 = \frac{\alpha_1 K_{1*}^{(2)} A + K_h^{(2)} B}{\alpha_1 A + B}; \qquad F_2 = \frac{\alpha_2 K_{1*}^{(2)} A + K_h^{(2)} B}{\alpha_2 A + B};$$

$$A = (K_h^{(1)} - K_{\text{sat}}^{(1)})(K_{1*}^{(1)} - K_h^{(1)}); \quad B = (K_{1*}^{(1)} - K_{\text{sat}}^{(1)})(K_h^{(2)} - K_{1*}^{(2)});$$

$$\alpha_1 = \frac{(K_{\min} - K_f^{(2)})^2 ((1-\phi)K_f^{(1)} - \phi K_{\min})^2}{(K_{\min} - K_f^{(1)})^2 ((1-\phi)K_f^{(2)} - \phi K_{\min})^2};$$

$$\alpha_2 = \alpha_1 \frac{K_f^{(2)}(3K_f^{(1)} + 4G_{\min})}{K_f^{(1)}(3K_f^{(2)} + 4G_{\min})};$$

$$K_h^{(1)} = \left[\frac{1-\phi}{K_{\min}} + \frac{\phi}{K_f^{(1)}}\right]^{-1}; \quad K_h^{(2)} = \left[\frac{1-\phi}{K_{\min}} + \frac{\phi}{K_f^{(2)}}\right]^{-1};$$

$$K_{1*}^{(1)} = (1-\phi)K_{\min} + \phi K_f^{(1)} - \frac{\phi(1-\phi)(K_{\min} - K_f^{(1)})^2}{\phi K_{\min} + (1-\phi)K_f^{(1)} + 4G_{\min}/3};$$

$$K_{1*}^{(2)} = (1-\phi)K_{\min} + \phi K_f^{(2)} - \frac{\phi(1-\phi)(K_{\min} - K_f^{(2)})^2}{\phi K_{\min} + (1-\phi)K_f^{(2)} + 4G_{\min}/3}.$$

Some properties of equation 10 are as follows:

1) The modulus F_1 is equivalent to Gassmann's prediction of saturated bulk modulus. F_1 corresponds to the smallest possible change in bulk modulus upon fluid substitution, which occurs when the rock pore space is well connected and the pore pressure ($P_p = -I_1/3$) can equilibrate under bulk compression.
2) The modulus F_2 corresponds to the largest possible change in bulk modulus upon fluid substitution. This occurs when the pore pressure is not uniform throughout the pore space under bulk compression — for example, when the rock pore space is disconnected or tight and has very heterogeneous pore stiffness (i.e., unrelaxed squirt flow).
3) If $K_f^{(1)} > 0$ and $K_{\text{sat}}^{(1)}$ is on either the HS+ or HS− bound, then upon fluid substitution to $K_f^{(2)} > 0$, $K_{\text{sat}}^{(2)} = F_1 = F_2$, is on the same corresponding bound for the new fluid; hence, fluid substitution for an initially saturated rock whose bulk modulus falls on a bound is unique.
4) If the initial case is dry ($K_f^{(1)} = 0$), and if $K_{\text{sat}}^{(1)}$ is on HS+ or HS− bound, then upon fluid substitution, F_1 is still Gassmann's prediction of the saturated rock bulk modulus and will lie on the same corresponding HS+ or HS− bound computed with the new fluid. If the dry $K_{\text{sat}}^{(1)}$ is on the HS− bound, then F_2 will be on the HS+ bound, and if the dry $K_{\text{sat}}^{(1)}$ is on the HS+ bound, then F_2 will stay on the HS+ bound.
5) If the initial case is dry ($K_f^{(1)} = 0$), and if $K_{\text{sat}}^{(1)}$ lies anywhere between (but not on) the HS− and HS+ bounds, then F_2 is the HS+ bound computed with the new fluid. If the initial rock is saturated, the prediction for dry modulus F_2 lies on HS−.

Next, we introduce physical realizations of the Gibiansky and Torquato (G&T) bounds.

SOLID SUBSTITUTION ON THE BOUNDS

For two-phase composites, the HS bounds, equations 8 and 9, are physically attainable by a multitude of microstructures (Hashin and Shtrikman, 1963; Milton, 1984a; Norris, 1985; Gibiansky and Sigmund, 2000). For example, the HS bound on the bulk modulus, but not the shear modulus, can be realized by a multiscale, space-filling pack of coated spheres. Milton (1984b) finds that the bulk and shear bounds can be realized simultaneously by certain multirank laminate geometries. The differential effective medium approach was shown by Norris (1985) to achieve the bounds on bulk and shear moduli simultaneously when the inclusions are disk shaped. Boucher (1974) and Norris (1985) pointed out that the nonsymmetric SC scheme of Wu (1966) for disk-shaped geometries attains both bounds when $(K_{\min} - K_f)(G_{\min} - G_f) \ge 0$. In this paper, we use the notation K_f and G_f for the bulk and shear moduli of the pore-filling material, either solid or fluid.

Although two-phase microgeometries exist that can attain the bounds on bulk modulus, but not the shear modulus, Berryman and Milton (1988) show that any two-phase microgeometry that attains the bounds on shear modulus must necessarily attain the bound on bulk modulus. Reviews on the subject of realizability of the bounds can be found in Gibiansky and Sigmund (2000), Norris (1985), Milton (2002), and Liu (2011).

The significance of realizability for this paper is the following. Because the bounds are realizable, there exist multiple two-phase microstructures for which equations 8 and/or 9 are the exact equations for the effective moduli of those materials. If either bulk or shear modulus of the initial composite, composed of solid or fluid phases with moduli ($K_{\min}$,$G_{\min}$) and ($K_f^{(1)}$, $G_f^{(1)}$), falls on the upper or lower bound, then when pore phase ($K_f^{(1)}$, $G_f^{(1)}$) is replaced by another solid or fluid phase ($K_f^{(2)}$, $G_f^{(2)}$), the corresponding moduli of the new composite are again on the respective bounds, as long as $(K_{\min} - K_f^{(1)})(G_{\min} - G_f^{(1)}) \ge 0$ and $(K_{\min} - K_f^{(2)})(G_{\min} - G_f^{(2)}) \ge 0$. That is, microstructures whose corresponding moduli fall exactly on a bound represent a class of materials for which we can perform liquid and solid substitution, exactly and uniquely.

Examples of the solid substitution on the bounds are shown in Figure 1. Figure 1a corresponds to a two-phase rock with quartz mineralogy ($K_{\min} = 36$ GPa, $G_{\min} = 45$ GPa) and solid pore fill with moduli $K_f^{(1)} = 3$ GPa and $G_f^{(1)} = 2$ GPa. Points $A^{(1)}$ and $B^{(1)}$ correspond to two realizable composites whose bulk moduli fall along the upper and lower bounds, respectively. Figure 1b corresponds to the same quartz mineralogy but a different pore-filling material with moduli $K_f^{(2)} = 2$ GPa and $G_f^{(2)} = 1$ GPa. The substitution of the pore fill causes the composites at $A^{(1)}$ and $B^{(1)}$ to move with the bounds and transform to $A^{(2)}$ and $B^{(2)}$, respectively.

As mentioned earlier, in this paper, we use the terms porosity and *pore volume fraction* to mean the volume fraction of the pore-filling material, even if it is a solid. In the remainder of the discussion, we will also use superscript (1) to indicate properties before substitution, and (2) to indicate properties after substitution.

An exception to the uniqueness of the substitution on the bounds occurs when the shear moduli of all initial phases are equal, causing

the initial upper and lower bounds to coincide, as in Figure 2. In this case, the point $A^{(1)}$ (Figure 2a) corresponds to a composite with calcite mineralogy ($K_{\min} = 72$ GPa, $G_{\min} = 32$ GPa) and solid pore fill with the bulk modulus $K_f^{(1)} = 30$ GPa and the same shear modulus $G_f^{(1)} = 32$ GPa. Upon substitution with a pore fill with moduli $K_f^{(2)} = 30$ GPa and $G_f^{(2)} = 0$ GPa, the upper and lower bounds separate (Figure 2b). The new composite modulus at point $A^{(2)}$ could fall on or anywhere between the bounds, depending on the pore geometry. Another exception is the degenerate case when the initial pore-filling material is identical to the grain material.

SOLID SUBSTITUTION OF BULK MODULUS USING EMBEDDED BOUNDS

Because equations 8 and 9 are physically realizable, we can embed the realizations recursively to represent additional pore space geometries and to calculate exactly, but not uniquely, the change in effective bulk modulus upon either solid or fluid substitution in the pore space.

The HS bounds plotted in Figure 3a show the range of possible bulk moduli for rocks composed of quartz mineralogy ($K_{\min} =$ 36 GPa, $G_{\min} = 45$ GPa) and solid pore fill ($K_f^{(1)} = 1$ GPa and $G_f^{(1)} = 0.5$ GPa) . Point $X^{(1)}$ represents one rock with porosity $\phi_X = 0.2$ and bulk modulus $K_X^{(1)} = 15$ GPa. Points $P^{(1)}$ ($\phi_P = 0.098$; $K_P^{(1)} = 30.89$ GPa; $G_P^{(1)} = 36.80$ GPa) and $Q^{(1)}$ ($\phi_Q = 0.303$; $K_Q^{(1)} = 4.32$ GPa; $G_Q^{(1)} = 2.73$ GPa) fall on the upper and lower and bounds, respectively. We choose porosities ϕ_P and ϕ_Q so that a HS+ bound constructed from the materials $P^{(1)}$ and $Q^{(1)}$ passes through point X:

$$K_X^{(1)} = K_P^{(1)} + \frac{f_Q}{(K_Q^{(1)} - K_P^{(1)})^{-1} + f_P\left(K_P^{(1)} + \frac{4}{3}G_P^{(1)}\right)^{-1}}, \quad (11)$$

where f_P is the volume fraction of material $P^{(1)}$ and $f_Q = (1 - f_P)$ is the volume fraction of material $Q^{(1)}$, such that $\phi_X = f_P\phi_P + f_Q\phi_Q$. (For a given ϕ_P, the ϕ_Q that satisfies equation 11 is found numerically; see Appendix A.) With this construction, $K_X^{(1)}$ is the modulus of a realizable composite of materials $P^{(1)}$ and $Q^{(1)}$, which in turn, are realizable composites of the mineral and pore-fill materials. Therefore, equation 11 is the exact expression for multiple microgeometries that have modulus $K_X^{(1)}$ at porosity 0.2.

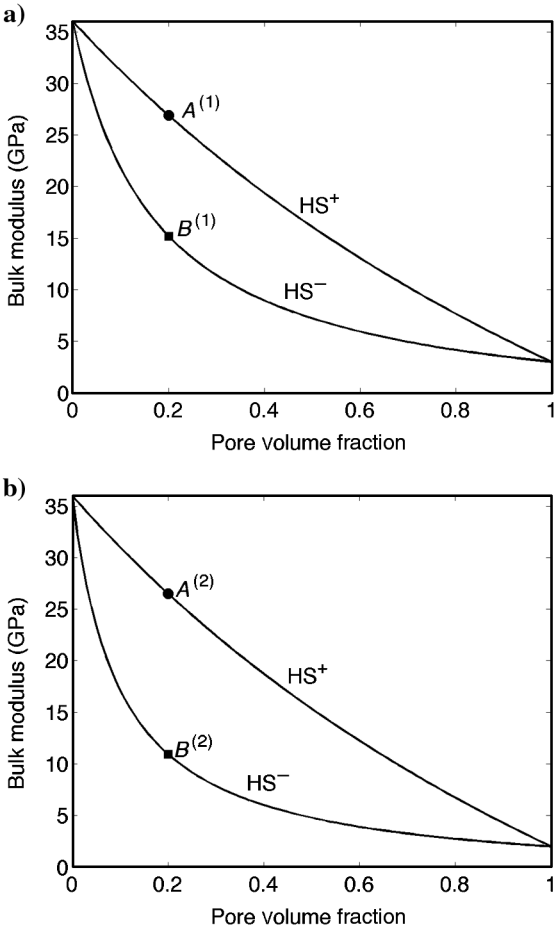

Figure 1. HS bounds on bulk modulus. (a) Example for quartz mineral with pore-filling moduli $K_f^{(1)} = 3$ GPa and $G_f^{(1)} = 2$ GPa. (b) Example for quartz mineral with pore-filling moduli $K_f^{(2)} = 2$ GPa and $G_f^{(2)} = 1$ GPa. Materials that happen to fall on the bulk modulus bounds, points $A^{(1)}$ and $B^{(1)}$, transform to points $A^{(2)}$ and $B^{(2)}$.

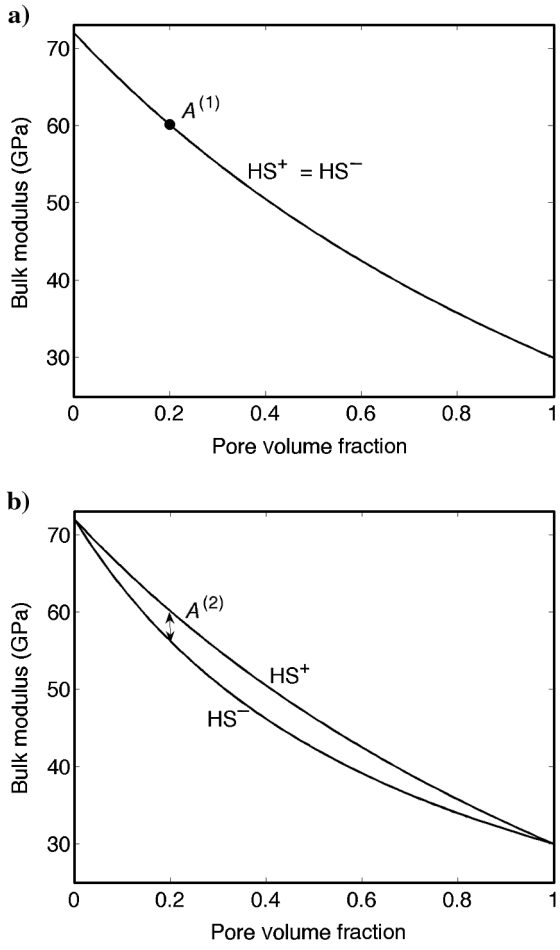

Figure 2. HS bounds on bulk modulus. (a) Example for calcite mineral ($K_{\min} = 72$ GPa, $G_{\min} = 32$ GPa), with pore-filling moduli $K_f^{(1)} = 30$ GPa and $G_f^{(1)} = 32$ GPa. (b) The same mineral with pore-filling moduli $K_f^{(2)} = 30$ GPa and $G_f^{(2)} = 0$ GPa.

Figure 3b shows the corresponding plot of bulk moduli when the solid pore fill ($K_f^{(1)} = 1$ GPa and $G_f^{(1)} = 0.5$ GPa) is replaced by a different solid pore fill ($K_f^{(2)} = 3$ GPa, $G_f^{(2)} = 2$ GPa). Upon solid substitution, the original points $P^{(1)}$ and $Q^{(1)}$ are transformed to points $P^{(2)}$ and $Q^{(2)}$, respectively, lying on the new bounds at the same porosities ϕ_P and ϕ_Q; the upper bound connecting points $P^{(1)}$ and $Q^{(1)}$ is transformed, as well. The bulk modulus $K_X^{(2)}$ at point $X^{(2)}$ corresponds to the original rock with the solid pore fill replaced by the new solid. Hence, $K_X^{(2)}$ is an exact (though nonunique) prediction of the bulk modulus after substituting one solid pore fill with another solid pore fill:

$$K_X^{(2)} = K_P^{(2)} + \frac{f_Q}{(K_Q^{(2)} - K_P^{(2)})^{-1} + f_P\left(K_P^{(2)} + \frac{4}{3}G_P^{(2)}\right)^{-1}}. \quad (12)$$

Although all of the constructions of the type discussed in Figure 3 are based on the same HS equations, in this paper we refer to the absolute HS bounds to indicate mixtures of the mineral and pore-fill end members, and modified HS bounds or *embedded bounds* to indicate embedded mixtures, such as that between materials at points $P^{(1)}$ and $Q^{(1)}$.

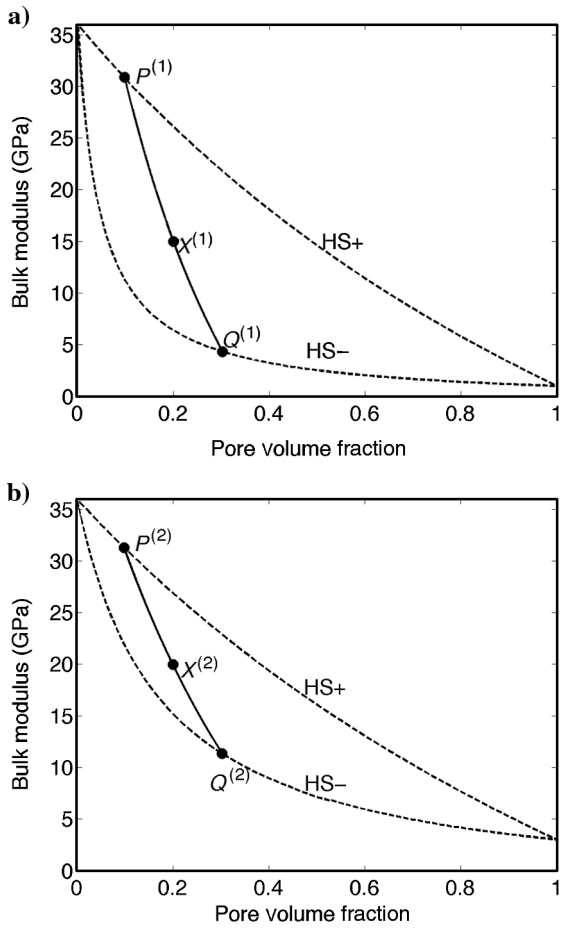

Figure 3. Substitution of solid pore fill ($K_f^{(1)} = 1$ GPa and $G_f^{(1)} = 0.5$ GPa) with a different solid pore fill ($K_f^{(2)} = 3$ GPa, $G_f^{(2)} = 2$ GPa) using a modified upper HS bound construction. Quartz mineral in frame. (a) Dashed curves are absolute bounds for initial composition. Data point $X^{(1)}$ falls between the bounds, but it can be physically realized by an HS+ composite consisting of end members at $P^{(1)}$ and $Q^{(1)}$. (b) With new composition, the absolute bounds shift. Points $P^{(1)}$ and $Q^{(1)}$ move to $P^{(2)}$ and $Q^{(2)}$, respectively. The same realizable microgeometry used to fit $X^{(1)}$ leads to the exact prediction $X^{(2)}$ at the new composition.

The intrinsic nonuniqueness of the solid substitution is illustrated in Figure 4. Figure 4a describes the same composition as in Figure 3a. The gray lines show some of the infinite number of modified upper HS realizations of point $X^{(1)}$ constructed from various pairs $P_i^{(1)}$ and $Q_i^{(1)}$. The corresponding predictions of the composite bulk modulus when the solid pore fill is replaced by the new solid pore fill are shown in Figure 4b. Each construction of the original point $K_X^{(1)}$ transforms to a slightly different $K_X^{(2)}$ upon substitution of the pore material. That is, upon solid substitution, the bulk modulus can take on a range of possible values, which depends on the (usually unknown) underlying microstructure.

Figure 5 shows limiting cases of the constructions described in Figure 4. In Figure 5a, curve ($A_{\min} - G^{(1)}$) and curve ($A_{\min} - D^{(1)}$) are modified upper and lower HS bound constructions from the mineral point $A_{\min}$ passing through the point $X^{(1)}$. We refer to these

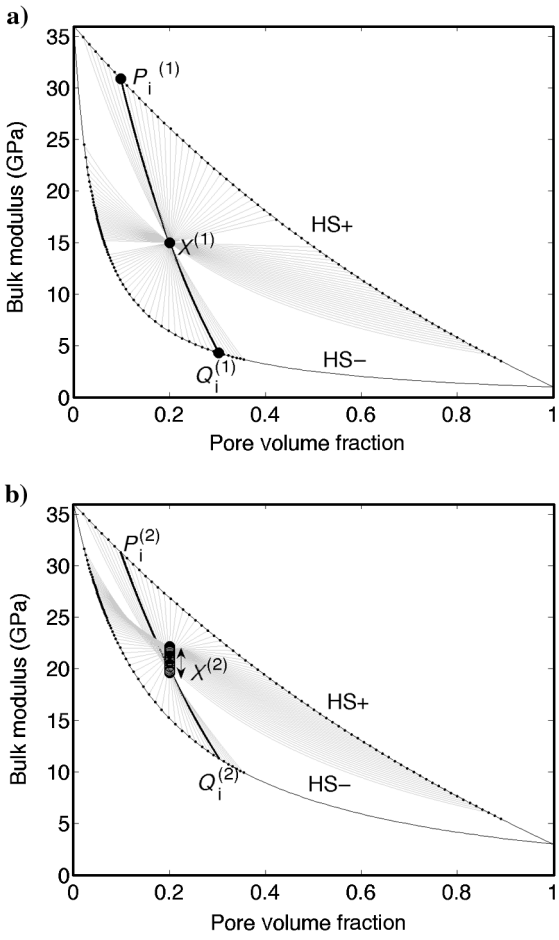

Figure 4. Similar to Figure 3 — substitution of solid pore fill ($K_f^{(1)} = 1$ GPa and $G_f^{(1)} = 0.5$ GPa) with a different solid pore fill ($K_f^{(2)} = 3$ GPa, $G_f^{(2)} = 2$ GPa). Data point $X^{(1)}$ can be physically realized by an infinite number of HS composites of end members at $P_i^{(1)}$ and $Q_i^{(1)}$ spanning along the upper and lower bounds, respectively. The range of realizable microgeometries used to fit $X^{(1)}$ leads to a range of predicted $X^{(2)}$ at the new composition.

as the HS^+_{min} and HS^-_{min} constructions, respectively. Curve $(A_f^{(1)} - E^{(1)})$ and curve $(A_f^{(1)} - B^{(1)})$ are HS+ and HS− constructions from the pore-fill point, $A_f^{(1)}$, passing through the point $X^{(1)}$. We refer to these as the HS^+_f and HS^-_f constructions, respectively. Curve $(C^{(1)} - H^{(1)})$ shows HS+ and HS− constructions from the upper and lower bounds at the data porosity 0.2. Figure 5b shows the same constructions after replacing the solid pore-filling material with the second solid pore-filling material.

From numerical examples, we conjecture that the four embedded HS constructions (HS^+_{min}, HS^-_{min}, HS^+_f, HS^-_f) illustrated in Figure 5 bound the range of substituted moduli $K_X^{(2)}$ that can be achieved with this class of embedded HS realizations. We have not found a rigorous proof that this is always so. However, we discuss in the next section that the HS^+_{min} and HS^-_f predictions of $K_X^{(2)}$ reduce to the G&T bounds when the pore fills are fluids.

Closed-form expressions for the solid-to-solid substitution using HS^+_{min} and HS^-_f are given in Appendix B. Strategies for numerical construction of the HS^-_{min} and HS^+_f are given in Appendix A. Note that HS^+_{min} and HS^-_f are independent of the shear moduli at points $G^{(1)}$ and $B^{(1)}$, and therefore, their predictions of bulk modulus are uncoupled from the shear modulus at point $X^{(1)}$. In contrast, HS^-_{min} and HS^+_f do depend on the shear moduli at points $D^{(1)}$ and $E^{(1)}$, respectively.

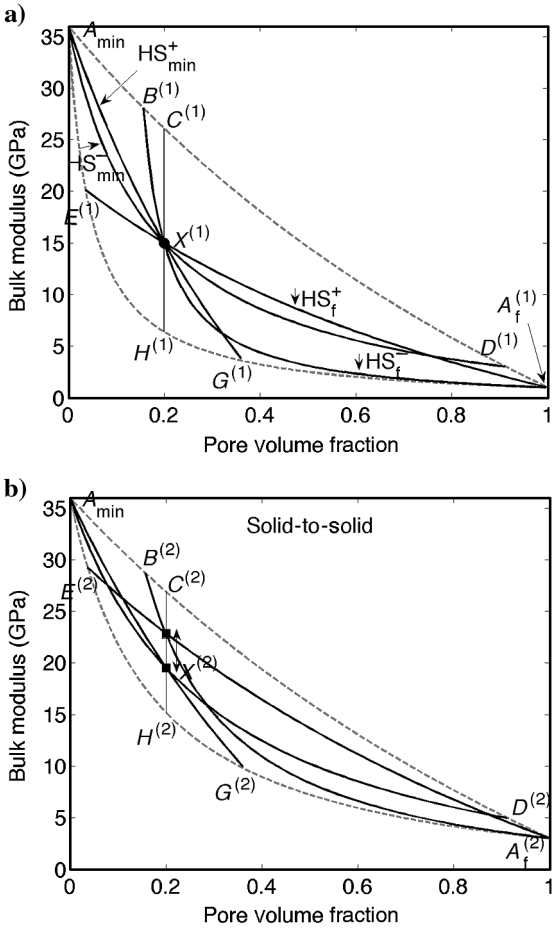

Figure 5. Substitution of solid pore fill ($K_f^{(1)} = 1$ GPa and $G_f^{(1)} = 0.5$ GPa) with a different solid pore fill ($K_f^{(2)} = 3$ GPa, $G_f^{(2)} = 2$ GPa). (a) Data point $X^{(1)}$ is realized by modified HS+ and HS− bounds passing from the mineral and pore-fill end members. (b) Substituting the pore fill from solid to liquid leads to a range of possible results $X^{(2)}$.

PROPERTIES OF THE EMBEDDED HS BOUND CONSTRUCTIONS WHEN THE PORE FILLS ARE FLUIDS

We now return to the problem of fluid substitution. We show that the HS^+_{min} and HS^-_f predictions defined in the previous section reduce to the G&T bounds, illustrating that those bounds are optimum.

Figure 6 shows the bulk modulus for rocks of quartz mineralogy and pore space filled with fluids. In Figure 6a, the pore fluid has moduli $K_f^{(1)} = 1$ GPa and $G_f^{(1)} = 0$. The embedded bound constructions in Figure 6 are the same as described earlier: The HS^+_{min} curve is the modified HS+ mix of the mineral point A_{min} and the absolute lower bound point $G^{(1)}$. Similarly, the HS^-_{min} curve is the modified HS− mix of the mineral point A_{min} and the absolute upper bound point $D^{(1)}$. When the pore fill is a fluid (or dry), the HS^+_{min}-constructed substitutions of $K_X^{(1)}$ to $K_X^{(2)}$ can be shown, with some algebra, to be exactly the same as Gassmann's prediction —

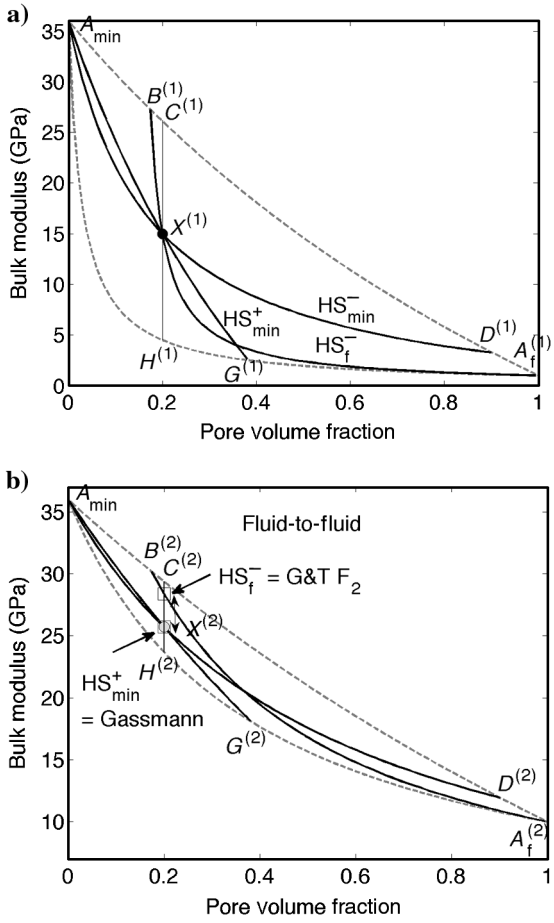

Figure 6. Substitution of fluid pore fill ($K_f^{(1)} = 1$ GPa and $G_f^{(1)} = 0$) with a different fluid pore fill $K_f^{(2)} = 10$ GPa and $G_f^{(2)} = 0$. (a) Data point $X^{(1)}$ is realized by modified HS+ and HS− bounds passing from the mineral point, as well as vertical HS bound. (b) Substituting the pore fluid leads to a range of possible results.

or the G&T bound for the smallest possible change in bulk modulus. (The HS^-_{min} fluid substitution is also exactly equal to Gassmann's prediction, if the shear modulus at point $D^{(1)}$ is also on the upper HS bound.) A coated-sphere realization of the HS^+_{min} constructions is illustrated in Figure 7. We see that for this choice of microstructure, the fluid phase always occurs in inclusions of the same shape (shells in Figure 7a). We emphasize that there are numerous microgeometries, other than spheres, that also correspond to the embedded HS constructions.

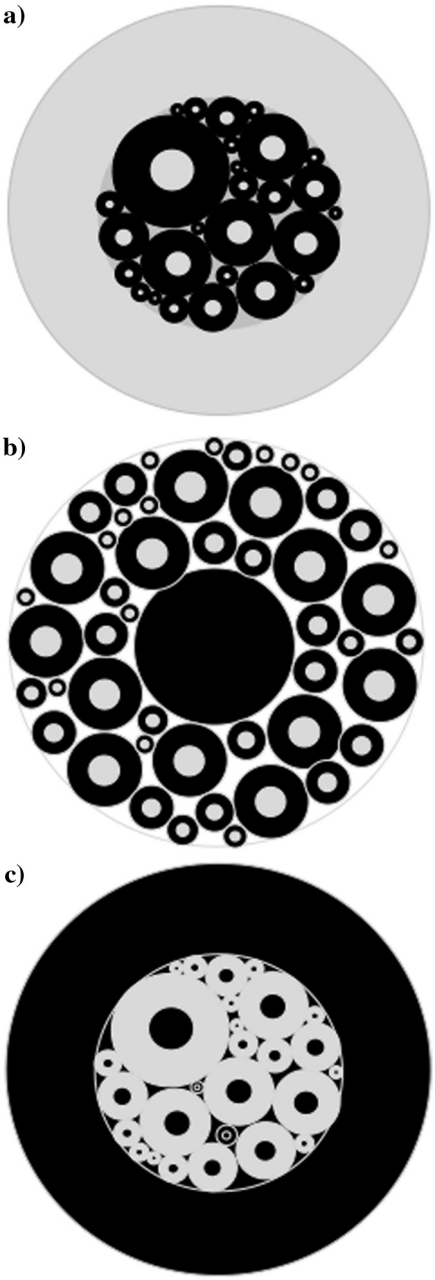

Figure 7. Coated-sphere realizations of the constructions in Figures 5 and 6. Black represents the pore-filling material. (a) The HS^+_{min} — mix of mineral point and lower bound point G. (b) The HS^+_f — mix of fluid point and lower bound point E. (c) The HS^-_f — mix of pore-fill point and upper bound point B.

When the pore-filling material is a fluid (zero shear modulus), the construction of the HS^-_f from the pore-fluid point $A^{(1)}_f$ through point $X^{(1)}$ is the same as the G&T second bound, F_2. This can also be proved algebraically. A coated-sphere realization of this construction is shown in Figure 7c.

When the pore-filling material is a fluid (zero shear modulus), the HS^+_f construction from the pore-fluid point $A^{(1)}_f$ to any point on the lower bound stays on the lower bound. Point $X^{(1)}$ cannot be realized in this way, unless it is on the lower bound. A coated-sphere example realization of this construction is shown in Figure 7b.

In summary, the embedded bound constructions represent physical realizations of the G&T bounds when the pore-filling materials are fluids. This illustrates that the G&T bounds are optimum.

MARION'S BOUND AVERAGE METHOD

The vertical black lines in Figures 5, 6, and 8 represent constructions of data point $X^{(1)}$ from composites of point $C^{(1)}$ on the absolute upper bound and point $H^{(1)}$ on the absolute lower bound; $C^{(1)}$

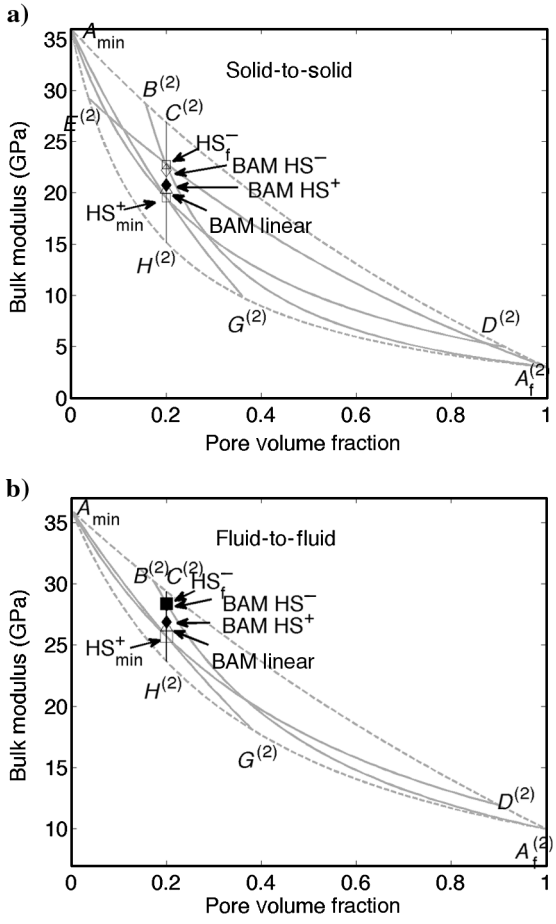

Figure 8. Comparison of BAMHS predictions with the modified HS constructions. (a) Substitution of solid pore fill ($K^{(1)}_f = 1$ GPa, $G^{(1)}_f = 0.5$ GPa) with a different fluid pore fill ($K^{(2)}_f = 3$ GPa, $G^{(2)}_f = 2$ GPa). (b) Substitution of liquid pore fill ($K^{(1)}_f = 1$ GPa, $G^{(1)}_f = 0$ GPa) with a different fluid pore fill ($K^{(2)}_f = 10$ GPa, $G^{(2)}_f = 0$ GPa). Effective moduli measured with the initial composition are $K^{(1)}_X = 15$ GPa and $G^{(1)}_X = 18$ GPa.

and $H^{(1)}$ lie at the same porosity ϕ_X as the data point $X^{(1)}$. Using equation 8, $K_X^{(1)}$ can be constructed as a modified HS+ mix of the materials at point $C^{(1)}$ ($K^{\mathrm{HS}+}$, $G^{\mathrm{HS}+}$) and point $H^{(1)}$ ($K^{\mathrm{HS}-}$, $G^{\mathrm{HS}-}$), such that the fraction of material $C^{(1)}$ is f^+ and the fraction of material $H^{(1)}$ is $(1-f^+)$. Alternatively, the data point $K_X^{(1)}$ can be constructed as an HS− mix of the materials at point $C^{(1)}$ ($K^{\mathrm{HS}+}$, $G^{\mathrm{HS}+}$) and point $H^{(1)}$ ($K^{\mathrm{HS}-}$, $G^{\mathrm{HS}-}$), such that the fraction of material $C^{(1)}$ is f^- and the fraction of material $H^{(1)}$ is $(1-f^-)$. The fractions are given by

$$f^+ = \frac{\frac{1}{K_X+(4/3)G^{\mathrm{HS}+}} - \frac{1}{K^{HS+}+(4/3)G^{\mathrm{HS}+}}}{\frac{1}{K^{\mathrm{HS}-}+(4/3)G^{\mathrm{HS}+}} - \frac{1}{K^{\mathrm{HS}+}+(4/3)G^{\mathrm{HS}+}}}, \tag{13}$$

$$f^- = \frac{\frac{1}{K_X+(4/3)G^{\mathrm{HS}-}} - \frac{1}{K^{\mathrm{HS}+}+(4/3)G^{\mathrm{HS}-}}}{\frac{1}{K^{\mathrm{HS}-}+(4/3)G^{\mathrm{HS}-}} - \frac{1}{K^{\mathrm{HS}+}+(4/3)G^{\mathrm{HS}-}}}. \tag{14}$$

After substituting the pore-filling material (fluid or solid), the absolute bounds are recomputed to yield the materials at points $C^{(2)}$ and $H^{(2)}$. Finally, the substituted modulus is computed by once again constructing the HS+ and HS− mixes using fractions f^+ and f^-, respectively.

These modified HS constructions at constant porosity resemble the bound average method (BAM) introduced by Marion and Nur (1991). In that work, Marion and Nur construct the starting data point $K_X^{(1)}$ as an arithmetic average (Voigt bound) of moduli on the absolute upper Voigt and lower Reuss bounds. They predicted the change in elastic moduli upon solid or liquid substitution in the pore space by taking the same arithmetic average after recomputing the upper and lower bounds for the new composition. Le Ravalec and Guéguen (1996) compared the BAM parameters with the differential SC model and poroelastic theory. Yan and Han (2011) further discuss the linear BAM approximation. We refer to the present constructions as the BAMHS+ and BAMHS− method of solid or fluid substitutions.

Figure 8a illustrates our BAMHS solid-to-solid substitution (the same parameters as in Figure 5); Figure 8b illustrates fluid-to-fluid substitution (same parameters as in Figure 6). The BAMHS predictions are shown by diamonds; the $\mathrm{HS}^+_{\mathrm{min}}$, $\mathrm{HS}^-_{\mathrm{min}}$, HS^+_f, and HS^-_f predictions are marked with squares. The BAMHS predictions again illustrate the nonuniqueness of the substituted bulk modulus, although they do not span the entire range of predicted $K_X^{(2)}$ as the $\mathrm{HS}^+_{\mathrm{min}}$, $\mathrm{HS}^-_{\mathrm{min}}$, HS^+_f, and HS^-_f constructions. The linear BAM prediction is shown by the triangle. For these examples, the linear BAM prediction lies close to the $\mathrm{HS}^+_{\mathrm{min}}$ prediction, which represents the smallest change in modulus upon substitution. The equations for predicting the solid substitution using the BAMHS method are much simpler than for the other constructions (see Appendix A). These, however, imply that the effective shear moduli at points $C^{(2)}$ and $H^{(2)}$ are also on the bounds, which may be restricted by measured shear data.

DISCUSSION

Figure 9 compares the modified bound solid-substitution predictions with those of Ciz and Shapiro (equations 6 and 7), again using the same material parameters as in Figure 5. As mentioned earlier, the C&S approximation of bulk modulus (equation 6) represents

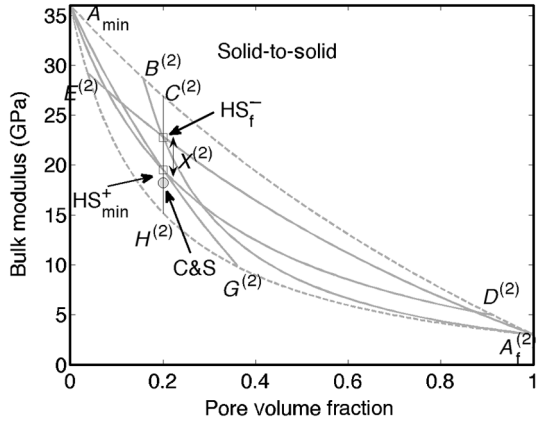

Figure 9. Comparison of the C&S approximation with the modified HS constructions. Substitution of solid pore fill ($K_f^{(1)} = 1$ GPa, $G_f^{(1)} = 0.5$ GPa) with a different solid pore fill ($K_f^{(2)} = 3$ GPa, $G_f^{(2)} = 2$ GPa). Effective moduli measured with the initial composition are $K_X^{(1)} = 15$ GPa and $G_X^{(1)} = 18$ GPa.

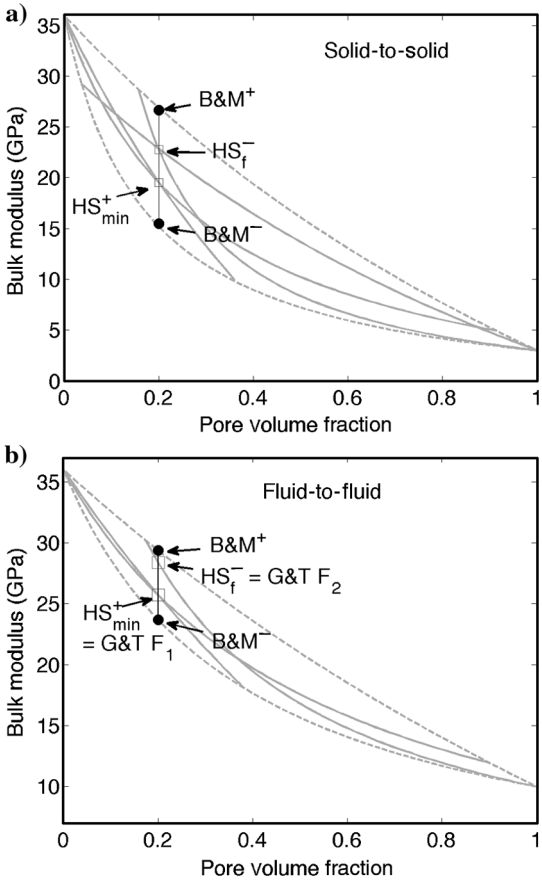

Figure 10. Comparison of the B&M predictions with the modified HS constructions. (a) Substitution of solid pore fill ($K_f^{(1)} = 1$ GPa, $G_f^{(1)} = 0.5$ GPa) with a different solid pore fill ($K_f^{(2)} = 3$ GPa, $G_f^{(2)} = 2$ GPa). (b) Substitution of liquid pore fill ($K_f^{(1)} = 1$ GPa, $G_f^{(1)} = 0$ GPa) with a different fluid pore fill ($K_f^{(2)} = 10$ GPa, $G_f^{(2)} = 0$ GPa). Effective moduli before substitution are $K_X^{(1)} = 15$ GPa and $G_X^{(1)} = 18$ GPa.

situations in which there is no change to the pore fill shear modulus upon solid substitution and when the mean stress within the pore-filling material is homogeneous under hydrostatic loading. Therefore, when $(K_f^{(1)} - K_f^{(2)})(G_f^{(1)} - G_f^{(2)}) \geq 0$ the C&S approximation usually underpredicts the change in the modulus upon substitution. In the case of Figure 9, the C&S prediction lies outside of the range defined by the modified bound constructions. In some cases, the C&S approximation predicts values lying outside of the absolute HS bounds.

Berryman and Milton (1988) discuss bounds (B&M) on elastic bulk and shear moduli that incorporate information about the three-point correlations of the pore space geometry. The geometric information makes the B&M bounds more restrictive than the HS bounds, and at least as tight as the bounds of Beran and Molyneux (1966). Using the B&M results, measured elastic moduli can be inverted for bounds on two parameters, which depend only on geometry. These parameters can, in turn, be used to put bounds on the elastic moduli if the pore-filling material is changed. Figure 10a compares solid-to-solid substitution using the B&M bounds with the HS_f^- and HS_{min}^+ constructions, for the same material parameters presented in Figure 5. Figure 10b compares fluid-to-fluid substitution using the B&M bounds, the HS_f^- and HS_{min}^+, and the G&T bounds, for the same material parameters presented in Figure 6. In Figure 10a and 10b, the B&M predictions are tighter than the HS bounds, but broader than the range spanned by the HS_f^- and HS_{min}^+ constructions. The HS_f^- and HS_{min}^+ and the G&T bounds are optimum for fluids.

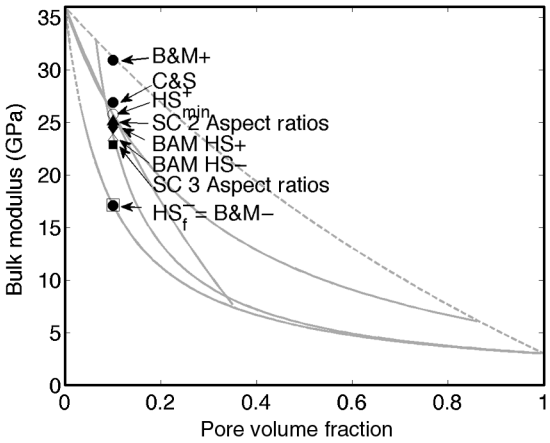

Figure 11. Comparison of the various solid substitution methods with examples computed using the SC approximation. Initial solid pore fill ($K_f^{(1)} = 3$ GPa, $G_f^{(1)} = 2$ GPa). Substituted pore fill is a liquid ($K_f^{(2)} = 3$ GPa, $G_f^{(2)} = 0$ GPa). Two-pore model has aspect ratios [1, 0.094]. Three-pore model has aspect ratios [1, 0.1, 0.001]. Effective moduli before substitution are $K_X^{(1)} = 26.9$ GPa and $G_X^{(1)} = 30.7$ GPa.

Figure 11 compares the various solid-substitution methods with examples of ellipsoidal-pore models computed using the SC approximation. The initial effective moduli are $K_X^{(1)} = 26.9$ GPa and $G_X^{(1)} = 30.7$ GPa. The initial pore fill is a solid ($K_f^{(1)} = 3$ GPa and $G_f^{(1)} = 2$ GPa). The substituted pore fill is a liquid ($K_f^{(2)} = 3$ GPa and $G_f^{(2)} = 0$ GPa). SC model parameters are shown in Table 2. The initial rock bulk and shear moduli are approximately fit with two different ellipsoidal-inclusion rock models — a stiff, monoporosity model (pore-aspect ratio 0.1; mineral-aspect ratio 1) and a dual-porosity model containing a mixture of cracks and stiff pores (pore-aspect ratios 0.1 and 0.001; mineral-aspect ratio 1). Upon substitution, the homogeneous, monoporosity model predicts a small change in bulk modulus $\Delta K \approx 1.8$ GPa, whereas the dual-porosity model with cracks predicts a change of $\Delta K \approx 4$ GPa. The modulus changes predicted by the SC model are bounded by the HS_f^- and HS_{min}^+ predictions. The C&S approximation predicts no change in bulk modulus because it ignores the pore-fill shear modulus.

Table 2. Parameters used in SC calculations displayed in Figure 11.

Solid-filled ($K_{fill} = 3.0$ GPa; $G_{fill} = 2$ GPa) to liquid-filled ($K_{fill} = 3.0$ GPa; $G_{fill} = 0$ GPa)

SC[2] solid-filled	Aspect ratio[3]	ϕ	SC[4] liquid-filled
$K_{dry} = 26.9$	[1, 0.1, 0.001]	0.1	$K_{eff} = 22.9$
	—	[0.9, 0.097, 0.003][5]	$G_{eff} = 12.6$
$G_{dry} = 30.7$	[1, .1]	0.1	$K_{eff} = 25.1$
	—	[0.9, 0.10]	$G_{eff} = 26.1$

[2]Solid-filled rock moduli computed using the SC approximation.
[3]Aspect ratios used in SC modeling: grain first, then pores.
[4]Liquid-filled rock moduli, computed using the SC approximation.
[5]Volume fractions; grain first then pores.

CONCLUSIONS

For materials whose bulk and/or shear moduli fall on the HS bounds, fluid or solid substitution is exact and unique. For composites that fall between the bounds, fluid substitution of the bulk modulus is not unique: Gassmann's prediction yields the smallest possible change, whereas the largest possible change is predicted by the G&T bounds. Changes in modulus larger than predicted by Gassmann can be caused by disconnected pores or unrelaxed pore pressure gradients that can be associated with large fluid viscosities and/or high measurement frequencies.

Solid substitution of bulk moduli can be computed exactly, but not uniquely for points between the bounds. The embedded bound constructions shown in this paper yield exact answers because they are the proper equations for bulk modulus, based on realizable materials. However, every initial bulk modulus can be realized with an infinite number of microstructures and therefore transforms to an infinite number of moduli upon substitution of the pore fill.

Our four limiting embedded bound constructions numerically appear to span the range of possible transformed bulk moduli. In the limiting case of pore fluids, two of these constructions reduce to the bounds of G&T, which illustrates that the G&T bounds are optimum. We also derive the HS equivalent of Marion's bounding average method (BAMHS). BAMHS predictions also reveal the nonuniqueness of solid and fluid substitution and are easy to implement, but they do not span the entire range of nonuniqueness revealed by the other methods.

This work illustrates that fluid substitution and solid substitution cannot be performed uniquely without detailed information about the pore space. If the pore space is well connected such that wave-induced pore fluid pressures are equilibrated, then Gassmann's equations are appropriate and are equal to G&T's lower bound, as well as the modified bound, HS^{+}_{min}, prediction.

Disconnected pores, or unequilibrated fluid pressures cause larger changes in modulus upon fluid substitution, which are bounded by the HS^{-}_{f} prediction as well as G&T's upper bound. As has been shown in previous work, the unequilibrated pore pressure has a much larger effect on modulus than unequilibrated viscous shear stress.

Solid substitution is inherently nonunique without detailed knowledge of the pore space geometry. The C&S approximation for bulk modulus represents the situation when the shear modulus of the pore-filling material remains unchanged, and induced mean stress in the pore space is homogeneous. The C&S approximation works best when pore space is stiff and homogeneous, and it tends to underpredict the change in bulk modulus upon solid substitution. The HS^{+}_{min} prediction in this paper also corresponds to relatively homogeneous pore stiffness. The presence of cracks and soft-grain contacts leads to larger changes in bulk modulus upon solid substitution.

Many effective medium models used in rock physics are geometry specific. These include sphere-pack models for unconsolidated sediments, ellipsoidal-inclusion models for consolidated sediments, contact cement models for early diagenesis, and crack models for fractured rocks. Such models yield useful quantitative predictions that often fit observations.

Geometry-specific models yield unique predictions of modulus change with fluid or solid substitution. However, these predictions can be misleading, because geometry-specific models are almost always gross idealizations of actual pore microstructure. We have shown in this paper that a measurement of elastic modulus and porosity can be fit with an infinite number of geometric models; each will yield a different prediction of solid (and possibly fluid) substitution. Uncertainty in these predictions can only be improved when supported with additional information about the real pore space geometry.

ACKNOWLEDGMENTS

This work was supported by the Stanford Rock Physics and Borehole Geophysics project and DOE contract DE-FE0001159. The authors thank R. Sain, K. Bandyopadhyay, C. Morency, Y. Guéguen, and E. Slob for useful and constructive comments.

APPENDIX A

EQUATIONS FOR PREDICTING THE EMBEDDED BOUND SOLID AND FLUID SUBSTITUTIONS

We show here the equations for predicting the pore fill substitutions illustrated in Figures 5 and 6.

Begin by computing the absolute upper and lower HS bounds between the mineral (moduli $= K_{min}$, G_{min}) and the original pore-filling solid or fluid (moduli $= K_f^{(1)}$, $G_f^{(1)}$):

$$K^{HS+(1)}(\phi) = \left[\frac{\phi}{K_f^{(1)} + (4/3)G_{min}} + \frac{1-\phi}{K_{min} + (4/3)G_{min}}\right]^{-1} - (4/3)G_{min}, \tag{A-1}$$

$$G^{HS+(1)}(\phi) = \left[\frac{\phi}{G_f^{(1)} + z_{min}} + \frac{1-\phi}{G_{min} + z_{min}}\right]^{-1} - z_{min},$$
$$z_{min} = \frac{G_{min}}{6}\left(\frac{9K_{min} + 8G_{min}}{K_{min} + 2G_{min}}\right), \tag{A-2}$$

$$K^{HS-(1)}(\phi) = \left[\frac{\phi}{K_f^{(1)} + (4/3)G_f^{(1)}} + \frac{1-\phi}{K_{min} + (4/3)G_f^{(1)}}\right]^{-1} - (4/3)G_f^{(1)}, \tag{A-3}$$

$$G^{HS-(1)}(\phi) = \left[\frac{\phi}{G_f^{(1)} + z_f^{(1)}} + \frac{1-\phi}{G_{min} + z_f^{(1)}}\right]^{-1} - z_f^{(1)},$$
$$z_f^{(1)} = \frac{G_f^{(1)}}{6}\left(\frac{9K_f^{(1)} + 8G_f^{(1)}}{K_f^{(1)} + 2G_f^{(1)}}\right). \tag{A-4}$$

The HS^{+}_{min} in Figures 5 and 6 is the modified upper HS bound between the mineral point and the absolute lower bound, passing through the input data point at porosity ϕ and original bulk modulus $K_{sat}^{(1)}$. The intersection of this curve with the absolute lower bound occurs at porosity ϕ_i:

$$\begin{aligned}\phi_i = &-\left\lfloor\left(4G_f^{(1)} + 3K_f^{(1)}\right)\left(K_{min} - K_{sat}^{(1)}\right)\right.\\ &\left.+\left(4G_f^{(1)} + 3K_{min}\right)\phi\left(K_f^{(1)} - K_{min}\right)\right\rfloor /\\ &\left\lfloor 3\left(K_{min} - K_{sat}^{(1)}\right)\left(K_{min} - K_f^{(1)}\right)\right\rfloor\\ &-\left\{\left(4G_f^{(1)} + 3K_{min}\right)\left[\left(4G_f^{(1)} + 3K_f^{(1)}\right)\left(K_{min} - K_{sat}^{(1)}\right)\right.\right.\\ &\left.\left.+\left(4G_f^{(1)} + 3K_{sat}^{(1)}\right)\phi\left(K_f^{(1)} - K_{min}\right)\right]\right\} /\\ &\left[12\left(G_{min} - G_f^{(1)}\right)\left(K_{min} - K_{sat}^{(1)}\right)\left(K_{min} - K_f^{(1)}\right)\right].\end{aligned} \tag{A-5}$$

Recompute the absolute lower bound for the new solid or fluid pore fill (moduli $= K_f^{(2)}$, $G_f^{(2)}$). The bulk modulus at porosity ϕ_i on the updated absolute lower bound is

$$K_i^{(2)} = \left[\frac{\phi_i}{K_f^{(2)} + (4/3)G_f^{(2)}} + \frac{1-\phi_i}{K_{min} + (4/3)G_f^{(2)}}\right]^{-1} - (4/3)G_f^{(2)}. \tag{A-6}$$

Finally, the new bulk modulus at the original porosity ϕ is

$$K_{\text{sat}}^{(2)} = \left[\frac{\phi/\phi_i}{K_i^{(2)} + (4/3)G_{\min}} + \frac{1-\phi/\phi_i}{K_{\min} + (4/3)G_{\min}}\right]^{-1} - (4/3)G_{\min}. \tag{A-7}$$

The curve HS_P^- is the modified lower HS bound between the pore-fill point and the absolute upper bound, passing through the input data point at porosity ϕ and original bulk modulus $K_{\text{sat}}^{(1)}$. The intersection of this curve with the absolute upper bound occurs at porosity ϕ_i:

$$\begin{aligned}\phi_i = {} & \left[\left(4G_{\min} + 3K_f^{(1)}\right)\left(4G_f^{(1)} + 3K_f^{(1)}\right)\right] / \\ & \left[12\left(G_{\min} - G_f^{(1)}\right)\left(K_{\min} - K_f^{(1)}\right)\right] \\ & - \left[\left(4G_{\min} + 3K_f^{(1)}\right)\left(4G_f^{(1)} + 3K_f^{(1)} - 4G_f^{(1)}\phi\right.\right. \\ & \left.\left. - 3K_{\text{sat}}^{(1)}\phi\right)\right] / \left[12\left(G_{\min} - G_f^{(1)}\right)\left(K_{\text{sat}}^{(1)} - K_f^{(1)}\right)\right].\end{aligned} \tag{A-8}$$

Recompute the absolute upper bound for the new solid or fluid pore fill (moduli $= K_f^{(2)}, G_f^{(2)}$). The bulk modulus at porosity ϕ_i on the updated absolute upper bound is

$$K_u^{(2)} = \left[\frac{\phi_i}{K_f^{(2)} + (4/3)G_{\min}} + \frac{1-\phi_i}{K_{\min} + (4/3)G_{\min}}\right]^{-1} - (4/3)G_{\min}. \tag{A-9}$$

Finally, the new bulk modulus at the original porosity ϕ is

$$K_{\text{sat}}^{(2)} = \left[\frac{(\phi-\phi_i)/(1-\phi_i)}{K_f^{(2)} + (4/3)G_f^{(2)}} + \frac{(1-\phi)/(1-\phi_i)}{K_u^{(2)} + (4/3)G_f^{(2)}}\right]^{-1} - (4/3)G_f^{(2)}. \tag{A-10}$$

The curve $\text{HS}_{\min}^-$ is the modified lower bound between the mineral point and the absolute upper bound, passing through the input data point at porosity ϕ and original bulk modulus $K_{\text{sat}}^{(1)}$. We have not found a simple closed-form expression analogous to equations A-5 and A-8, but we can solve numerically for the porosity ϕ_i at the intersection between the absolute upper bound, equation A-1, and the modified bound

$$K_{\text{sat}}^{(1)} = \left[\frac{\phi/\phi_i}{K_i^{(1)} + (4/3)G_i^{(1)}(\phi_i)} + \frac{1-\phi/\phi_i}{K_0 + (4/3)G_i^{(1)}}\right]^{-1} - (4/3)G_i^{(1)}, \tag{A-11}$$

where $K_i^{(1)} = K^{\text{HS}+(1)}(\phi_i)$ and $G_i^{(1)} = G^{\text{HS}+(1)}(\phi_i)$. Then evaluate the pore-substituted moduli $K_i^{(2)}$ and $G_i^{(2)}$ on the upper bound at porosity ϕ_i following equations A-1 and A-2. Finally, the new pore-substituted bulk modulus at the original porosity ϕ is

$$K_{\text{sat}}^{(2)} = \left[\frac{\phi/\phi_i}{K_i^{(2)} + (4/3)G_i^{(2)}} + \frac{1-\phi/\phi_i}{K_0 + (4/3)G_i^{(2)}}\right]^{-1} - (4/3)G_i^{(2)}. \tag{A-12}$$

The curve HS_f^+ is the modified upper bound between the pore-fill point and the absolute lower bound, passing through the input data point at porosity ϕ and original bulk modulus $K_{\text{sat}}^{(1)}$. We have not found a simple closed-form expression analogous to equations A-5 and A-8, but we can solve numerically for the porosity ϕ_i at the intersection between equation A-3 and the modified bound

$$\begin{aligned}K_{\text{sat}}^{(1)}(\phi_i) = {} & \left[\frac{(\phi-\phi_i)/(1-\phi_i)}{K^{\text{HS}-(1)}(\phi_i) + (4/3)G^{\text{HS}-(1)}(\phi_i)}\right. \\ & \left. + \frac{(1-\phi)/(1-\phi_i)}{K_f^{(2)} + (4/3)G^{\text{HS}-(1)}(\phi_i)}\right]^{-1} \\ & - (4/3)G^{\text{HS}-(1)}(\phi_i),\end{aligned} \tag{A-13}$$

where $K_i^{(1)} = K^{\text{HS}(1)}(\phi_i)$ and $G_i^{(1)} = G^{\text{HS}-(1)}(\phi_i)$. Then evaluate the pore-substituted moduli $K_i^{(2)}$ and $G_i^{(2)}$ on the absolute lower bound at porosity ϕ_i following equations A-3 and A-4. Finally, the new pore-substituted bulk modulus at the original porosity ϕ is

$$K_{\text{sat}}^{(2)} = \left[\frac{(\phi-\phi_i)/(1-\phi_i)}{K_i^{(2)} + (4/3)G_f^{(2)}} + \frac{(1-\phi)/(1-\phi_i)}{K_{\min} + (4/3)G_f^{(2)}}\right]^{-1} - (4/3)G_f^{(2)}. \tag{A-14}$$

APPENDIX B

CLOSED-FORM EXPRESSIONS FOR SUBSTITUTION

Starting with a solid or fluid saturated rock of original effective bulk modulus $K_{\text{sat}}^{(1)}$ (mineral moduli $= K_{\min}, G_{\min}$; original pore-filling moduli $= K_f^{(1)}, G_f^{(1)}$), the two embedded bounds on the effective bulk modulus upon substitution with a new pore solid or fluid (moduli $= K_f^{(2)}, G_f^{(2)}$) can be calculated as

$$\frac{K_{\text{sat}}^{(2)\text{HS}_{\min}^+}}{K_{\min} - K_{\text{sat}}^{(2)\text{HS}_{\min}^+}} = \frac{K_f^{(2)}}{\phi(K_{\min} - K_f^{(2)})} + \frac{4G_{\min}(G_f^{(2)} - G_f^{(1)}) + \Delta}{(G_{\min} - G_f^{(1)})(4G_f^{(2)} + 3K_{\min})}, \tag{B-1}$$

where

$$\Delta = \frac{4G_{\min}K_{\min}(G_f^{(1)} - G_f^{(2)}) + 3K_{\min}K_{bc}^{(1)}(G_{\min} - G_f^{(2)}) + 4G_f^{(2)}K_{bc}^{(1)}(G_{\min} - G_f^{(1)})}{(K_{\min} - K_{bc}^{(1)})}, \tag{B-2}$$

and

$$K_{bc}^{(1)} = \frac{K_{\text{sat}}^{(1)}\left(\frac{\phi K_{\min}}{K_f^{(1)}} + 1 - \phi\right) - K_{\min}}{\frac{\phi K_{\min}}{K_f^{(1)}} + \frac{K_{\text{sat}}^{(1)}}{K_{\min}} - 1 - \phi}, \tag{B-3}$$

$K_{\text{sat}}^{(2)\text{HS}_{\min}^+}$ is identical to the Gassmann or C&S prediction if $G_f^{(2)} = G_f^{(1)}$. Explicit expressions for $K_{\text{sat}}^{(2)\text{HS}_f^-}$ and $K_{\text{sat}}^{(2)\text{HS}_{\min}^-}$ are not presented here due to their complicated functional form, readers should calculate these using equations in Appendix A. Note that the difference between the upper and lower embedded bounds depends on the original effective bulk modulus.

If one instead starts with a dry or drained rock (effective dry bulk modulus $K_{\rm dry}$), then the lower embedded bound on the effective bulk modulus upon substitution with a new pore solid or fluid (moduli = K_f, G_f) is

$$K_{\rm sat}^{{\rm HS}^+_{\rm min}} = \frac{\phi\left(\frac{1}{K_{\rm min}} - \frac{1}{K_f}\right) + \left(\frac{1}{K_{\rm min}} - \frac{1}{K_{bc}}\right)}{\frac{\phi}{K_{bc}}\left(\frac{1}{K_{\rm min}} - \frac{1}{K_f}\right) + \frac{1}{K_{\rm min}}\left(\frac{1}{K_{\rm min}} - \frac{1}{K_{bc}}\right)}, \qquad \text{(B-4)}$$

where K_{bc} is

$$K_{bc} = \frac{(1-\phi)\left(\frac{1}{K_{\rm min}} - \frac{1}{K_{\rm dry}}\right) + \left(\frac{3\phi}{4}\right)\left(\frac{1}{G_{\rm min}} - \frac{1}{G_f}\right)}{\left(\frac{3\phi}{4}\right)\left(\frac{1}{K_{\rm min}G_{\rm min}} - \frac{1}{K_{\rm dry}G_f}\right) + \frac{1}{K_{\rm min}}\left(\frac{1}{K_{\rm min}} - \frac{1}{K_{\rm dry}}\right)}. \qquad \text{(B-5)}$$

Starting with a solid or fluid saturated rock (effective bulk modulus $K_{\rm sat}$) the two embedded bounds on the dry or drained bulk modulus are

$$K_{\rm dry}^{{\rm HS}^+_{\rm min}} = \frac{K_{bc}\left(\frac{1}{K_{\rm min}} + \frac{3\phi}{4G_f}\right) + \phi - 1}{\frac{K_{bc}}{K_{\rm min}}\left(\frac{1}{K_{\rm min}} + \frac{3\phi}{4G_{min}}\right) - \frac{(1-\phi)}{K_{\rm min}} + \frac{3\phi}{4}\left(\frac{1}{G_f} - \frac{1}{G_{\rm min}}\right)}, \qquad \text{(B-6)}$$

where K_{bc} in terms of K_{sat} is

$$K_{bc} = \frac{K_{\rm sat}\left(\frac{\phi K_{\rm min}}{K_f} + 1 - \phi\right) - K_{\rm min}}{\frac{\phi K_{\rm min}}{K_f} + \frac{K_{\rm sat}}{K_{\rm min}} - 1 - \phi}. \qquad \text{(B-7)}$$

REFERENCES

Beran, M. J., and J. Molyneux, 1966, Use of classical variational principles to determine bounds for the effective bulk modulus in heterogeneous media: Quarterly of Applied Mathematics, **24**, 107–118.

Berryman, J. G., 1980, Long-wavelength propagation in composite elastic media: Journal of the Acoustical Society of America, **68**, 1809–1831, doi: 10.1121/1.385171.

Berryman, J. G., and G. W. Milton, 1988, Microgeometry of random composites and porous media: Journal of Applied Physics D, **21**, 87–94, doi: 10.1088/0022-3727/21/1/013.

Biot, M. A., 1962, Mechanics of deformation and acoustic propagation in porous media: Journal of Applied Physics, **33**, 1482–1498, doi: 10.1063/1.1728759.

Boucher, S., 1974, On the effective moduli of isotropic two-phase elastic composites: Journal of Composite Materials, **8**, 82–89, doi: 10.1177/002199837400800108.

Brown, R., and J. Korringa, 1975, On the dependence of the elastic properties of a porous rock on the compressibility of the pore fluid: Geophysics, **40**, 608–616, doi: 10.1190/1.1440551.

Chapman, M., S. V. Zatsepin, and S. Crampin, 2002, Derivation of a microstructural poroelasticity model: Geophysical Journal International, **151**, 427–451, doi: 10.1046/j.1365-246X.2002.01769.x.

Ciz, R., and S. Shapiro, 2007, Generalization of Gassmann equations for porous media saturated with a solid material: Geophysics, **72**, no. 6, A75–A79, doi: 10.1190/1.2772400.

Gassmann, F., 1951, Über die Elastizität poröser Medien: Vierteljahrsschrift der Naturwissenschaftlichen Gesellschaft in Zürich, **96**, 1–23.

Gibiansky, L. V., and O. Sigmund, 2000, Multiphase composites with extremal bulk modulus: Journal of the Mechanics and Physics of Solids, **48**, 461–498, doi: 10.1016/S0022-5096(99)00043-5.

Gibiansky, L., and S. Torquato, 1998, Rigorous connection between physical properties of porous rocks: Journal of Geophysical Research, **103**, 23911–23923, doi: 10.1029/98JB02340.

Gurevich, B., D. Makarynska, and M. Pervukhina, 2009, Ultrasonic moduli for fluid-saturated rocks: Mavko-Jizba relations rederived and generalized: Geophysics, **74**, no. 4, N25–N30, doi: 10.1190/1.3123802.

Hashin, Z., and S. Shtrikman, 1963, A variational approach to the elastic behavior of multiphase materials: Journal of the Mechanics and Physics of Solids, **11**, 127–140, doi: 10.1016/0022-5096(63)90060-7.

Kanter, Y., and D. J. Bergman, 1984, Improved rigorous bounds on the effective elastic moduli of a composite material: Journal of the Mechanics and Physics of Solids, **32**, 41–62, doi: 10.1016/0022-5096(84)90004-8.

Le Ravalec, M., and Y. Guéguen, 1996, High- and low-frequency elastic moduli for a saturated porous/cracked rock — Differential self-consistent and poroelastic theories: Geophysics, **61**, 1080–1094, doi: 10.1190/1.1444029.

Liu, L., 2011, New optimal microstructures and restrictions on the attainable Hashin-Shtrikman bounds for multiphase composite materials: Philosophical Magazine Letters, **91**, 473–482, doi: 10.1080/09500839.2011.586373.

Marion, D., and A. Nur, 1991, Pore-filling material and its effect on velocity in rocks: Geophysics, **56**, 225–230, doi: 10.1190/1.1443034.

Mavko, G., and D. Jizba, 1991, Estimating grain-scale fluid effects on velocity dispersion in rocks: Geophysics, **56**, 1940–1949, doi: 10.1190/1.1443005.

Mavko, G., and T. Mukerji, 1995, Pore space compressibility and Gassmann's relation: Geophysics, **60**, 1743–1749, doi: 10.1190/1.1443907.

Mavko, G., and A. Nur, 1975, Melt squirt in the asthenosphere: Journal of Geophysical Research, **80**, 1444–1448, doi: 10.1029/JB080i011p01444.

Milton, G. W., 1984a, Microgeometries corresponding exactly with effective medium theories, *in* D. L. Johnson, and P. N. Sen, eds., Physics and chemistry of porous media: AIP Conference Proceedings 107, American Institute of Physics, 66.

Milton, G. W., 1984b Modeling the properties of composites by laminates: Presented at Workshop on Homogenization and Effective Moduli of Materials and Media, Institute for Mathematics and Its Applications.

Milton, G. W., 1986, Modeling the properties of composites by laminates, *in* J. L. Ericksen, D. Kinderlehrer, R. Kohn, and J.-L. Lions, eds., Homogenization and effective moduli of material and media: Springer-Verlag.

Milton, G. W., 2002, The theory of composites: Cambridge University Press.

Norris, A. N., 1985, A differential scheme for the effective moduli of composites: Mechanics of Materials, **4**, 1–16, doi: 10.1016/0167-6636(85)90002-X.

O'Connell, R., and B. Budiansky, 1977, Viscoelastic properties of fluid-saturated cracked solids: Journal of Geophysical Research, **82**, 5719–5735, doi: 10.1029/JB082i036p05719.

Stoll, R. D., and G. M. Bryan, 1970, Wave attenuation in saturated sediments: Journal of the Acoustical Society of America, **47**, 1440–1447, doi: 10.1121/1.1912054.

Torquato, S., 2001, Random heterogeneous materials: Microstructure and macroscopic properties: Springer.

Walpole, L., 1966, On bounds for the overall elastic moduli of inhomogeneous systems: Journal of the Mechanics and Physics of Solids, **14**, 151–162, doi: 10.1016/0022-5096(66)90035-4.

Wu, T. T., 1966, The effect of inclusion shape on the elastic moduli of a two-phase material: International Journal of Solids and Structures, **2**, 1–8, doi: 10.1016/0020-7683(66)90002-3.

Yan, F., and D.-H. Han, 2011, Theoretical validation of fluid substitution by Hashin-Shtrikman bounds: 81st Annual International Meeting, SEG, Expanded Abstracts, 2251–2255.

Zou, W., Q. He, J. Huang, and Q. Zheng, 2010, Eshelby's problem of non-elliptical inclusions: Journal of the Mechanics and Physics of Solids, **58**, 346–372, doi: 10.1016/j.jmps.2009.11.008.